Color Doppler Ultrasound and Gamma Imaging of Intratumorally Injected 500 nm Iron–Silica Nanoshells

Alexander Liberman,[†] Zhe Wu,[‡] Christopher V. Barback,[‡] Robert Viveros,[⊥] Sarah L. Blair,[¶] Lesley G. Ellies,[#] David R. Vera,[‡] Robert F. Mattrey,[‡] Andrew C. Kummel,[§] and William C. Trogler[§,*]

[†]Materials Science and Engineering Program, [‡]Department of Radiology, [§]Department of Chemistry and Biochemistry, [⊥]Department of Nanoengineering, [¶]Moores Cancer Center, and [#]Department of Pathology, University of California, San Diego, 9500 Gilman Drive, #0358 La Jolla, California 92093, United States

ABSTRACT Perfluoropentane gas filled iron-silica nanoshells have been developed as stationary ultrasound contrast agents for marking tumors to guide surgical resection. It is critical to establish their long-term imaging efficacy, as well as biodistribution. This work shows that 500 nm Fe—SiO_2 nanoshells can be imaged by color Doppler ultrasound over the course of 10 days in Py8119 tumor bearing mice. The 500 nm nonbiodegradable SiO_2 and biodegradable Fe—SiO_2 nanoshells were functionalized with diethylenetriamine pentaacetic acid (DTPA) ligand and radiolabeled with $^{111}In^{3+}$ for biodistribution studies in nu/nu mice. The majority of radioactivity was detected in the liver and kidneys following intravenous (IV) administration of nanoshells to healthy animals. By contrast, after nanoshells were injected intratumorally, most of the radioactivity remained at the injection site; however, some nanoshells escaped into circulation and were distributed similarly as those given intravenously. For intratumoral delivery of nanoshells and IV delivery to healthy animals, little difference was seen between the biodistribution of SiO_2 and biodegradable Fe—SiO_2 nanoshells. However, when nanoshells were administered IV to tumor bearing mice, a significant increase was observed in liver accumulation of SiO_2 nanoshells relative to biodegradable Fe—SiO_2 nanoshells. Both SiO_2 and Fe—SiO_2 nanoshells accumulate passively in proportion to tumor mass, during intravenous delivery of nanoshells. This is the first report of the biodistribution following intratumoral injection of any biodegradable silica particle, as well as the first report demonstrating the utility of DTPA-^{111}In labeling for studying silica nanoparticle biodistributions.

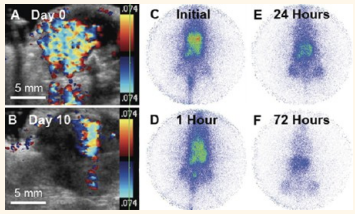

KEYWORDS: nanoparticles · ultrasound · scintigraphy · silica · biodistribution

Silica nanoparticles have been applied to bioimaging, drug delivery, and therapeutic sensitization owing to their ease of synthesis, high surface area, well-established surface modification chemistry and high *in vivo* stability.[1−7] Silica microshells and nanoshells have been studied for applications in ultrasound imaging, both as contrast agents and sensitizing agents in high intensity focused ultrasound.[8−13] Martinez *et al.* showed that perfluoropentane filled hollow silica and silica–boron microshells could be used as an effective color Doppler ultrasound contrast agent in tissue samples.[9] Ta *et al.* demonstrated that systemically administered silica nanoshells and microshells could be potentially used to outline well vascularized late stage ovarian tumors *in vivo* using contrast pulse sequencing contrast ultrasound imaging.[10] Hu *et al.* showed that even without a perfluorocarbon agent, it is possible to achieve substantial enhancement of ultrasound contrast using silica microshells when injected within the testicle of a rat.[12] Lin *et al.* have also demonstrated that tetraethoxysilane (TEOS) derived hollow silica shell particles can be used as ultrasound contrast agents *in vitro* with contrast pulse sequencing imaging, and that the acoustic properties of the particles depend on shell thickness and material properties.[13] One potential application of silica nanoparticles is in improving current surgical techniques used to mark tumors for removal in breast conservation therapy.

Many breast tumors are nonpalpable during surgery; consequently, the current standard for intraoperative identification during breast conservation therapy is to resect around a preoperatively implanted guidewire.[14] However, wire guidance is often problematic resulting in a need for second surgeries. This is due to incomplete resection because the wire often moves during surgery and does not localize tumor margins effectively in three dimensions.[14,15]

* Address correspondence to wtrogler@ucsd.edu.

Received for review May 17, 2013 and accepted June 26, 2013.

Published online June 26, 2013
10.1021/nn402507d

Furthermore, guide wire insertion is painful and must be done the day of surgery while the patient is conscious, thereby creating logistical expense for care providers and causing stress to the patient.

An alternative method of intraoperative guidance is the use of radioactive seed localization. Radioactive seeds are injected preoperatively using imaging guidance. Subsequently, the surgeon uses a gamma counter as a guide to extract the tumor. Gray *et al*. have demonstrated that the use of radioactive seed localization can decrease the rate of reoperation because of positive margins by up to 62%.[16] Similarly, Hughes et al. found that the negative margin rate increased up to 73% from 54% when comparing radioactive seed localization to wire localization.[17] Unfortunately, radioactive seed localization is less commonly employed due to the radiation exposure to the patient and the personnel. The shielded radioactive seed requires a painful incision for insertion through a tube or large hollow needle.

Ultrasound imaging is being explored as a means to improve breast tumor resection. Ultrasound is a low cost real time imaging tool that is commonly used in operating rooms.[15,18−21] Rahusen *et al*. found that in lumpectomies when ultrasound guidance was used, 89% of patients had a negative margin compared with 55% of patients when wire localization was used.[15] However, only a subpopulation of tumors can be visualized with standard ultrasound imaging based on the tumor morphology and specific type of cancer. Some cancers can only be visualized by MRI or by the presence of microcalcifications observed during mammography.[20] These tumors tend to have positive margins more often because they are more likely to have invasive components.[22]

Perfluoropentane vapor filled hollow 500 nm iron-silica nanoshells have been developed as an alternative means of marking tumors for standard ultrasound guided surgery. It is proposed that the nanoshells would be injected preoperatively into the tumors using the same image-guidance technique that is employed with guide-wires or radioactive seeds. Injection would use a fine syringe needle to reduce patient discomfort; afterward, color Doppler ultrasound imaging during surgery would guide the surgeon to and around the tumor for complete resection. The iron−silica nanoshells are stationary markers that can be used to mark multiple foci for resection, pose no risk to the personnel, and can be injected several days before surgery, thereby overcoming critical deficiencies of guide wires and radioactive seeds. The nanoshells can be employed for all patients, and even those whose tumors cannot be imaged by standard ultrasound imaging.

In studying the biodistribution of silica nanoparticles, He *et al*. reported that IV administered 45 nm surface modified silica nanoparticles could be excreted through renal clearance in mice as shown by transmission electron microscopy (TEM) and energy dispersive spectroscopy (EDS) of mouse urine.[23] Lu *et al*. reported the *in vivo* tolerance, biodistribution, and drug delivery capability of ∼100 nm mesoporous silica nanoparticles;[7] they reported that IV dosing of 50 mg/kg caused very little to no overt reaction and at least 90% of such a dose could be excreted in the urine and feces over 96 h. Furthermore, ICP−MS biodistribution experiments showed that the highest concentrations of these 100 nm mesoporous silica nanoparticles at 48 h were in the lungs and the implanted tumors. Conversely, Lui *et al*. observed in mice with 100 nm mesoporous hollow silica nanoparticles that after an IV dose of 80 mg/kg, 85% of the injected dose accumulated primarily in the spleen and the liver after 24 h. This dropped to 60% over the course of 1 week.[24] Detectable traces of the particles could be found even 1 month after injection in the liver, spleen, kidneys, and brain by ICP-OES. Wang *et al*. used perfluorohexane liquid filled ∼300 nm mesoporous hollow silica nanoshells and found that after an IV dose of 12 mg/rabbit the number of nanoshells detected in the tumor tripled over 24 h (10−33 ng/mg of Si), while after 24 h spleen, liver, and lungs all retained between 35 and 50 ng/mg of Si. Small amounts of nanoshells could be detected in the kidneys throughout the 24 h study (less than 10 ng/mg).[11] Decuzzi *et al*. measured the biodistribution by ICP−AES of spherical silica particles ranging from 700 nm to 3000 nm in size; it was reported that for IV injections, as particle size increased, the percentage of the injected dose of particles accumulating in non-RES organs decreased.[25] Of the total injection, ∼1% of 700 nm particles were detected in the kidneys at a high dose of particles, as well as approximately 4% of 1000 nm particles were detected at a low dose indicating that the biodistribution of particles can have dose dependent variability. These previous studies show that the silica nanoparticle/nanoshell biodistribution is sensitive to their size, composition, processing, payload, and injection site. A study of the biodistribution of biodegradable Fe−SiO_2 nanoshells is critical for their eventual application as a stationary marker for tumor resection. The goal is to determine what fraction of nanoshells injected intratumorally remain within the injection site, and to determine the fate of those that do not remain within the injection site.

This study describes the application of Fe−SiO_2 nanoshells as stationary ultrasound contrast markers, as well as the biodistribution of diethylenetriamine pentaacetic (DTPA)-^{111}In functionalized Fe−SiO_2 nanoshells to quantify intratumoral particle retention efficiency. DTPA-^{111}In labeling provides an effective method for studying particle biodistributions in a variety of systems over an extended period of time due to a relatively long ^{111}In half-life (2.81 days) and high detection sensitivity. Therefore, DTPA-^{111}In

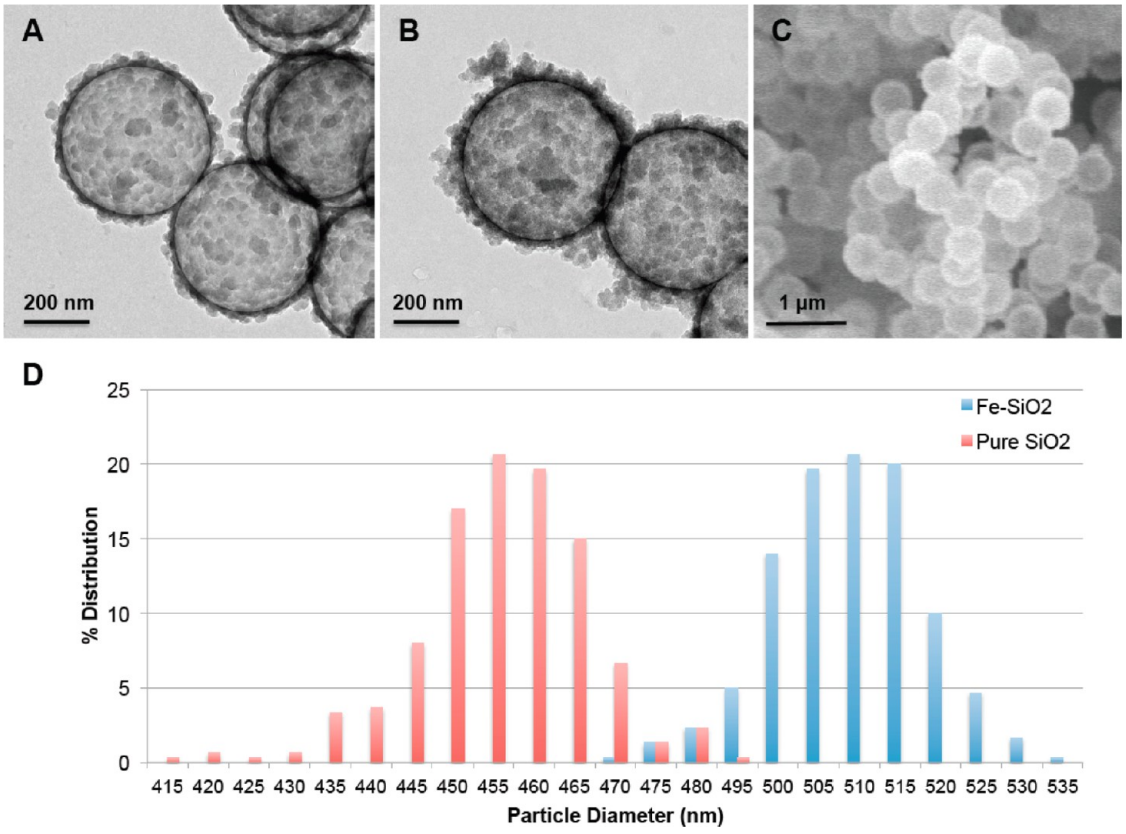

Figure 1. Electron microscopy of nanoshells. (A) TEM image of pure silica nanoshells shows that the nanoshells are hollow. Scale bar is 200 nm. (B) TEM image of Fe−SiO_2 nanoshells, which exhibit a thicker shell, show more dark regions and increased surface colloidal matter. (C) SEM image of Fe−SiO_2 nanoshells, which shows the high degree of sample uniformity. (D) Size distribution for Fe−SiO_2 and SiO_2 nanoshells. The average size and standard deviation of Fe−SiO_2 nanoshells was found to be 512 ± 9 nm; the average size and standard deviation for pure SiO_2 nanoshells was found to be 458 ± 11 nm.

labeling has found use to dynamically observe biodistributions.[26−28] Kommerredy *et al.* studied various DTPA-^{111}In labeled 220−250 nm gelatin particles to determine the rate of blood clearance and biodistribution.[26] It was found that the amount of particles observed in the kidneys increased for 48 h from ~20% up to 50% of the injected activity/gram tissue, which was attributed to breakdown and disintegration of gelatin nanoparticles. Zhang *et al.* have used DTPA-^{111}In to study the targeting potential and biodistribution of peptide targeted core cross-linked polymeric micelles to EphB4 receptors in a xenograft model of prostate cancer.[27] The efficacy of this targeting moiety was established by demonstrating an increase in accumulation compared to untargeted particles and by competitive inhibition of targeting binding sites by co-dosing with the targeting moiety. Despite the relative increase in targeting, it was observed that less than 3% injected dose/gram was retained by the tumors. The majority of particles were retained by the liver and the spleen (between 15 and 25% injected dose/gram for each organ). DTPA has been previously conjugated onto the surface of silica nanoparticles for magnetic resonance imaging with chelated Gd^{3+}.[3,5,29]

RESULTS AND DISCUSSION

The present study explores the use of surface anchored DTPA for chelating $^{111}In^{3+}$ to define the biodistribution of silica and biodegradable silica nanoshells. It has been shown that for gas filled silica microshells and nanoshells, that larger particles generate greater ultrasound contrast with imaging modalities such as contrast pulse sequencing.[8] Larger particles are also desirable for application as stationary ultrasound contrast markers to reduce escape from the site of implantation. Biodegradable 100 and 200 nm Fe−SiO_2 nanoshells have been synthesized, but the synthetic method was limited to these smaller sizes.[30,31] To increase the particle diameter to 500 nm for use as stationary markers in tissue, the quantity of TMOS per given mass of polystyrene templates was reduced in order to account for the reduction in relative surface area of templates due to the increase in diameter. Additionally, the reaction time was extended in order to allow for the mechanically less stable iron-silica coating to grow a thicker wall, so it would not fracture during subsequent calcination. The resulting 500 nm Fe−SiO_2 nanoshells differ from 500 nm pure SiO_2 nanoshells in several ways by TEM (Figure 1A,B), the Fe−SiO_2 nanoshells have much thicker walls, more

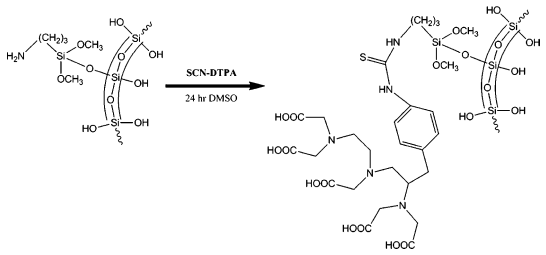

Scheme 1. Nanoshell functionalization with SCN-DTPA.

dark regions and increased surface colloidal matter. Nevertheless, the Fe−SiO_2 nanoshells appear to be uniform in bulk as seen by scanning electron microscopy (SEM) (Figure 1C). The nanoparticle size distribution seen in Figure 1D was determined from SEM image analysis; the average size and standard deviation of Fe−SiO_2 nanoshells was found to be 512 ± 9 nm, the average size and standard deviation for pure SiO_2 nanoshells was found to be 458 ± 11 nm. The iron content of the Fe−SiO_2 nanoshells, as determined by energy dispersive X-ray spectroscopy, was found to be 4.9 ± 1.5 mol %.

111-Indium is a useful short-lived gamma emitter for biodistribution studies.[26−28] DTPA has proven to be a useful ligand for complexing In(III) in biodistribution studies of gel particles,[26] and the approach is readily adapted for labeling silica based nanoparticles.[3,5,29] For example, silica and iron−silica nanoshells were functionalized with 3-aminopropyl triethoxysilane (3-APTES) in order to cover the surface of the nanoshell with amine groups for conjugation.[32] Excess 3-APTES was removed and the nanoshells were treated with DTPA−SCN (or FITC) as shown in Scheme 1. It is well-known that such isothiocyanates will react with primary amines to surface anchor DTPA or fluorescein.[33,34] The nanoshells functionalized with DTPA, were then radiolabeled by incubation with aqueous $^{111}InCl_3$. It was observed by dose calibrator that nanoshells which were not functionalized with DTPA did not retain any radioactivity after centrifugation and washing.

For application in breast conservation surgery, the goal envisioned is to preoperatively inject these particles by image guidance in the same fashion that radioactive seeds or guide wires are implanted to help localize tumors precisely for resection. Therefore, it is critical that the particles remain stationary before and throughout surgery. As shown in the ultrasound color Doppler image in Figure 2A, particles injected next to a tumor margin in mastectomy tissue are not transported away from site of localization (also confirmed by cross-sectional fluorescence microscopy). This property allows multiple injections around the tumor to thoroughly outline the margin. Figure 2B is a fluorescence microscopy image of a cross-sectional cut through the injection site. The fluorescence was from fluoroscein isothiocyanate (FITC) that was covalently linked to the surface of the particle; the fluorescence

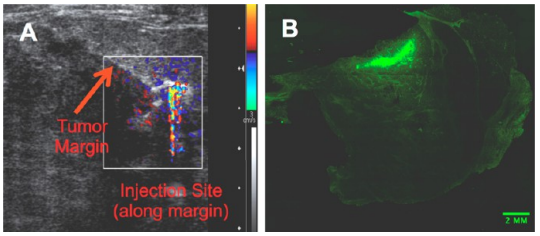

Figure 2. *Ex vivo* injection into excised mastectomy tissue. (A) Ultrasound color Doppler image from a 100 μL injection of gas filled 500 nm iron−silica FITC functionalized nanoshells into mastectomy tissue along the tumor margin. Note: asymmetric contrast was due to shadowing. (B) Fluorescence microscopy scan at 5× magnification through a cross-sectional cut of the injection site seen in image A. Green area is attributed to fluorescence from FITC conjugated onto the surface of the nanoshells.

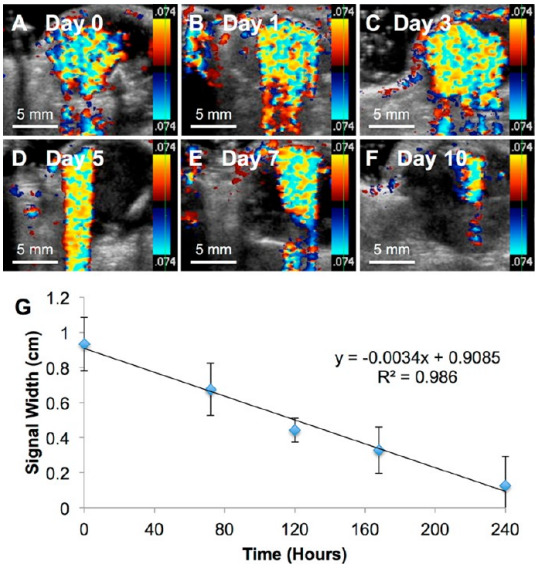

Figure 3. Intratumoral nanoshell ultrasound imaging longevity. Amounts of 50 μL of 500 nm PFP gas filled Fe−SiO_2 nanoshells at a concentration of 4 mg/mL were injected intratumorally into eight Py8119 tumor bearing mice and imaged by color Doppler imaging. The mechanical index was 1.9 with an imaging frequency of 7 MHz. (A) Imaging immediately after injection. (B) Imaging at 1 day postinjection. (C) Imaging at 3 days postinjection. (D) Imaging at 5 days postinjection. (E) Imaging at 7 days postinjection. (F) Imaging at 10 days postinjection. (G) Color Doppler signal width was measured and plotted vs time postinjection. Error bars signify standard deviations.

was restricted to an area of several square millimeters, which was consistent with the volume that was injected initially. This confirms the ultrasound imaging result that the particles are retained at the injection site with minimal diffusion.

To validate the application of these nanoshells as a local ultrasound guide marker for tumor resection *in vivo*, Fe-doped nanoshells were injected intratumorally into eight Py8119 tumor bearing nu/nu mice. The particles were imaged intermittently by color Doppler ultrasound over the course of 10 days (Figure 3A−F). The color Doppler signal width was measured and plotted against time (Figure 3G). It was found that

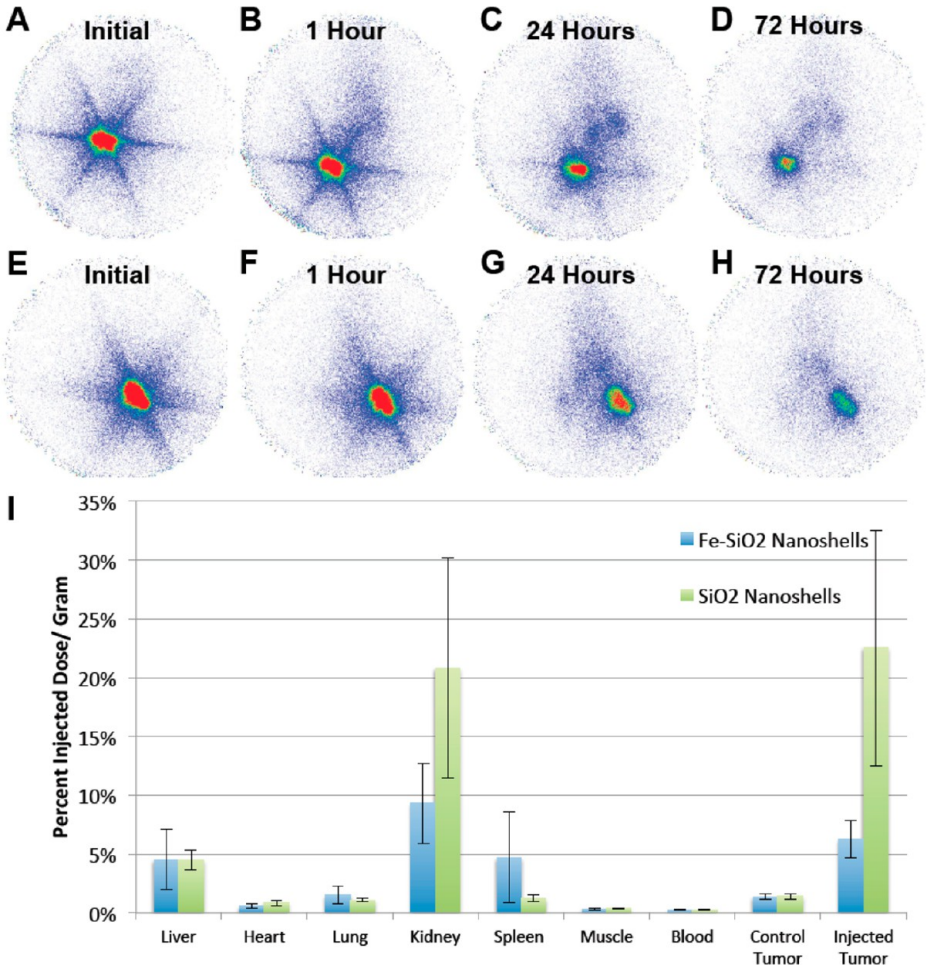

Figure 4. Biodistribution of 500 nm Fe−SiO_2 and SiO_2 nanoshells post intratumoral injection. Py8119 tumor bearing mice were injected intratumorally into a single tumor per mouse with 100 μL of DTPA-^{111}In labeled gas filled 500 nm Fe−SiO_2 nanoshells (A−D) and SiO_2 nanoshells (E−H) and imaged by gamma scintigraphy. (A) Imaging during the injection. (B) Imaging 1 h postinjection. (C) Imaging 24 h postinjection. (D) Imaging 72 h postinjection. (E) Imaging during the injection. (F) Imaging 1 h postinjection. (G) Imaging 24 h postinjection. (H) Imaging 72 h postinjection. (I) Gamma counter readings of harvested organs and tumors for Fe−SiO_2 and SiO_2 nanoshells. Error bars are of the standard deviation.

the signal persisted for 10 days and decayed linearly with imaging over time. It has been shown that perfluorocarbon gas filled nanoshells have mechanical subpopulations that can be imaged at various ultrasound mechanical index outputs.[8] To maximize the number of simultaneous nanoshells being imaged, a higher mechanical index (1.9) (ultrasound power) was applied. As a result of using a higher mechanical index, a substantial degree of shadowing was observed from the high reflectivity of the particles. This shadowing was observed under ultrasound as an exaggerated color Doppler tail, which embellishes the color Doppler signal along the *Y*-axis (Figure 3D). This shadowing is a well-understood behavior of ultrasound imaging. To overcome interference from the observed shadowing, the signal width was used to measure the signal decay over time instead of the signal area. As can be seen from Figure 3 A−F, the nanoshells were well retained by the Py8119 tumor and could be successfully imaged over the course of 10 days. Moreover, as seen in Figure 3G, the signal width was found to decay linearly over time. It is hypothesized that the relatively large size and rigidity of these particles dramatically reduces their diffusion through relatively dense tissue and the extracellular matrix.[35]

To determine biodistributions, Fe−SiO_2 and SiO_2 nanoshells were functionalized with DTPA and were radiolabeled with ^{111}In. Nanoshells were injected intratumorally into a single tumor per mouse (each mouse carried two tumors) and planar γ-scintigraphic imaging was performed as shown in Figure 4A−H. After 72 h, animals were sacrificed, the organs were harvested, and radioactivity was measured with the γ-counter. As can be seen from the scintigraphic images in Figure 4A−H, particles appear to be well retained at the injection site in the tumor. Note the particles cover a larger volume for the SiO_2 nanoshells since that particular tumor was slightly larger than the tumor used for the Fe−SiO_2 nanoshells. Analysis of individual organs by γ-counting (Figure 4I) showed the

SiO_2 nanoshells were slightly better retained by the injected tumors, and for both types of nanoshells there was substantial activity in other organs. The activity in the liver and the spleen were expected as these organs are associated with filtration of particulates, and some are expected to escape due to the relatively large size of the injection volume (100 μL) compared to the size of the tumor (~1000 mm^3). The radioactivity observed in the kidney was unexpected since it has been stated by Longmore *et al.* that larger particles (~8 nm or larger) cannot readily be excreted by the kidneys due to the structure and pore size throughout the kidney.[36] However, as previously stated the biodistribution is sensitive to the nanoparticle size, composition, processing, and injection conditions. For example, Lu *et al.* using ~100 nm mesoporous silica nanoparticles found that more than 90% could be excreted in the urine and feces over 96 h,[7] and Decuzzi *et al.* were able to detect 1000 nm solid silica nanoparticles in the kidneys by ICP–AES; therefore, it is possible that some particles are present within the kidneys.[25] Alternatively, the radioactivity observed in the kidney may arise from shell fragments or surface degradation of the nanoshells and subsequent release and renal filtration of the ^{111}In-DTPA complex similar to the effect that was observed by Kommerredy *et al.* with degradable gelatin nanoparticles.[26] The effect on biodistribution of free *versus* bound ^{111}In-DTPA has been studied by Paik *et al.* using antibodies. It was determined that when ^{111}In-DTPA was linked to antibodies with cleavable disulfide and diester linkages compared to noncleavable linkers, the cleaved ^{111}In-DTPA complexes had an accelerated clearance from circulation in rats.[37] Another example of rapid clearance of free ^{111}In-DTPA has been demonstrated in Wistar rats. Only 2 h after intravenous administration of ^{111}In-DTPA the largest retained dose was found in the kidneys, which only retained an average 0.126% injected dose/gram.[38] Li *et al.* found that when studying the biodistribution of ^{111}In-DTPA in mammary tumor bearing mice, the ^{111}In-DTPA was cleared rapidly from the blood with insignificant retention in the tumors.[39] Overall, ^{111}In-DTPA alone is not well retained *in vivo* and rapidly cleared through the renal system unless it is anchored by a macromolecule or particle that is not readily cleared. As a result, it is likely that the radioactive signal retained by the animals over the course of 72 h in the present work is predominantly due to indium retained by surface anchored DTPA on nanoshells. Furthermore, as seen in Figure 4E there was also a strong signal in the kidney from the nonbiodegradable pure SiO_2 nanoshells, which is more consistent with the kidneys retaining some of the nanoshells. Free $^{111}In^{3+}$ released from the chelator is known to bind plasma transferrin and follow a similar biodistribution as iron bound transferrin.[40] Therefore, free $^{111}In^{3+}$ would not be expected to remain largely confined to the injection site of nanoshells over the course of 72 h as it appears by scintigraphy.

The distribution of pure SiO_2 nanoshells appear to have a similar profile to the distribution of Fe–SiO_2 nanoshells for intratumoral delivery, but much more signal is retained by these particles especially in the injected tumor and in the kidneys. Part of this difference can be attributed to normalization by organ mass; for this experiment the tumors for the Fe–SiO_2 nanoshell injection were on average over double the mass compared to pure SiO_2 nanoshells. Another difference which can be accounted for is that in one of the injections of Fe–SiO_2 nanoshells, a vessel was nicked almost immediately during the intratumoral injection, which partially delivered some particles systemically and shifted the average values and standard deviations, most noticeably in the case of the spleen. In well vascularized tumors, it is difficult to predict and avoid the vasculature when performing the intratumoral injections. For both particles, some signal was observed in the control tumors that received no direct injection.

Since a small fraction of nanoshells passively accumulate in the tumors during intratumoral delivery, the nanoshells were also administered intravenously in the same murine model to study their biodistribution and potential use in tumor detection using gamma imaging. Nanoshells were injected intravenously and planar γ-scintigraphic imaging was performed as shown in Figure 5A–H. After 72 h, animals were sacrificed, the organs were harvested, and total organ radioactivity was measured with the use of a γ-counter. Figure 5A shows that the particles are initially spread throughout the entire body of the animal with an initial high accumulation in the liver. However, even immediately after initial injection of the Fe–SiO_2 nanoshells seen in Figure 5A, an outline of the tumors (two bilateral lobes on the legs near the bottom of the mouse at the center of the image) can be observed at the bottom of the mouse. The tumor images become increasingly distinct over time in Figure 5C–D. It is hypothesized that the nanoparticles retained by the tumor are a product of the enhanced permeation and retention (EPR) effect which has been documented for various *in vivo* tumor models.[41–43] The poorly developed vasculature in the tumor sequesters and retains macromolecules and nanoparticles within the tumor due to poor circulation, drainage, and leakiness. The Fe–SiO_2 and the SiO_2 nanoshells had about the same amount of accumulation in the tumor as measured by scintigraphy. Furthermore, the amount of Fe–SiO_2 compared to the SiO_2 nanoshells retained by each tumor were approximately constant, when normalized by tumor mass, as evidenced by the nearly equal values of percent injected dose per gram tumor for both groups of particles (Figure 5I). With the exception of a larger signal strength in the liver, as seen in Figure 5E–I, the pure SiO_2 nanoshells exhibited a similar biodistribution

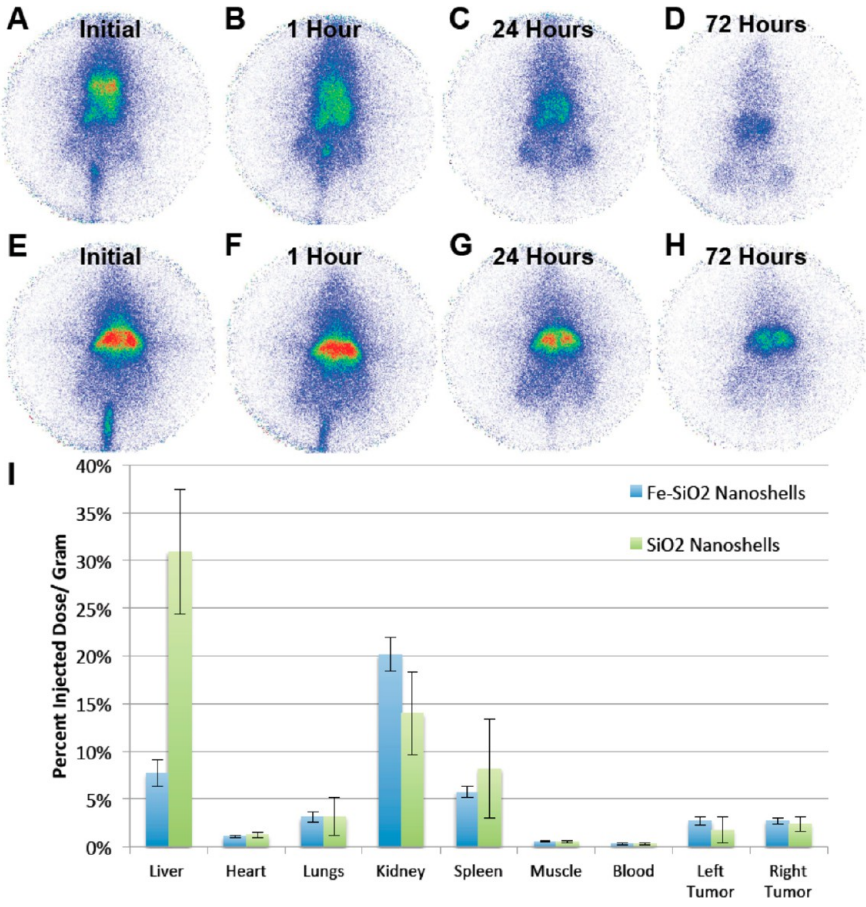

Figure 5. Biodistribution of radiolabeled 500 nm Fe−SiO_2 and SiO_2 nanoshells in Py8119 tumor bearing nu/nu mice with IV delivery. Py8119 tumor bearing mice were injected intravenously with 100 μL of ^{111}In labeled gas filled 500 nm Fe−SiO_2 nanoshells (A−D) and SiO_2 nanoshells (E−H) then imaged by gamma scinitigraphy. (A) Imaging during the injection. (B) Imaging 1 h postinjection. (C) Imaging 24 h postinjection. (D) Imaging 72 h postinjection. (E) Imaging during the injection. (F) Imaging 1 h postinjection. (G) Imaging 24 h postinjection. (H) Imaging 72 h postinjection. (I) Gamma counter readings of harvested organs and tumors for Fe−SiO_2 and SiO_2 nanoshells. Error bars are the standard deviations.

profile as the Fe−SiO_2 nanoshells. The enhanced liver signal for pure SiO_2 nanoshells compared to that of Fe−SiO_2 nanoshells was initially considered an aberration; however, verification by experimental repetition showed this to be consistent and not an artifact. Previous research has documented that extrahepatic tumors may significantly alter liver function.[44−48] It was found that even a tumor grown in the quadriceps of a mouse could have an impact on various hepatic receptors' expression and function, which can result in perturbed liver metabolism.[45] It is possible that the tumors grown could have affected the cell surface chemistry and retention of the nanoshells within the liver, which may account for the differences in particle retention observed. It was noted that the enhanced liver accumulation of pure SiO_2 nanoshells compared to Fe−SiO_2 nanoshells after IV injection was not observed in healthy mice (Figure 6). Alternatively, it is possible that the overall lower liver signal that is found in the Fe−SiO_2 nanoshells is due to the effects of biodegradation, which is further accentuated by the higher metabolic activity of rapidly growing tumor tissue. It has been hypothesized that the Fe−SiO_2 nanoshells degrade *via* transferrin-mediated pathway,[30] and it is known that many cancers overexpress transferrin receptors,[49−51] which may accelerate Fe−SiO_2 nanoshell degradation.

For ultimate clinical applications of Fe−SiO_2 nanoshells as stationary ultrasound guide markers, it is critical to establish whether adverse effects could occur if the particles were inadvertently administered intravenously or intra-arterially. It is also important to define the destination of particles that might leak from the tumor. To examine these scenarios, four healthy nu/nu mice per group were injected intravenously through the tail vein with 100 μL of ^{111}In labeled gas filled 500 nm Fe−SiO_2 and SiO_2 nanoshells and imaged by gamma scintigraphy. Whole animal scintigraphy showed that the majority of the Fe−SiO_2 nanoshells localize to the liver (Figure 6A−D). Organ γ-counting after sacrifice (Figure 6E), showed a substantial amount of signal in the kidneys and liver, but very little signal was detected elsewhere. The amount of signal in the kidneys shown in Figure 6E appears higher than in

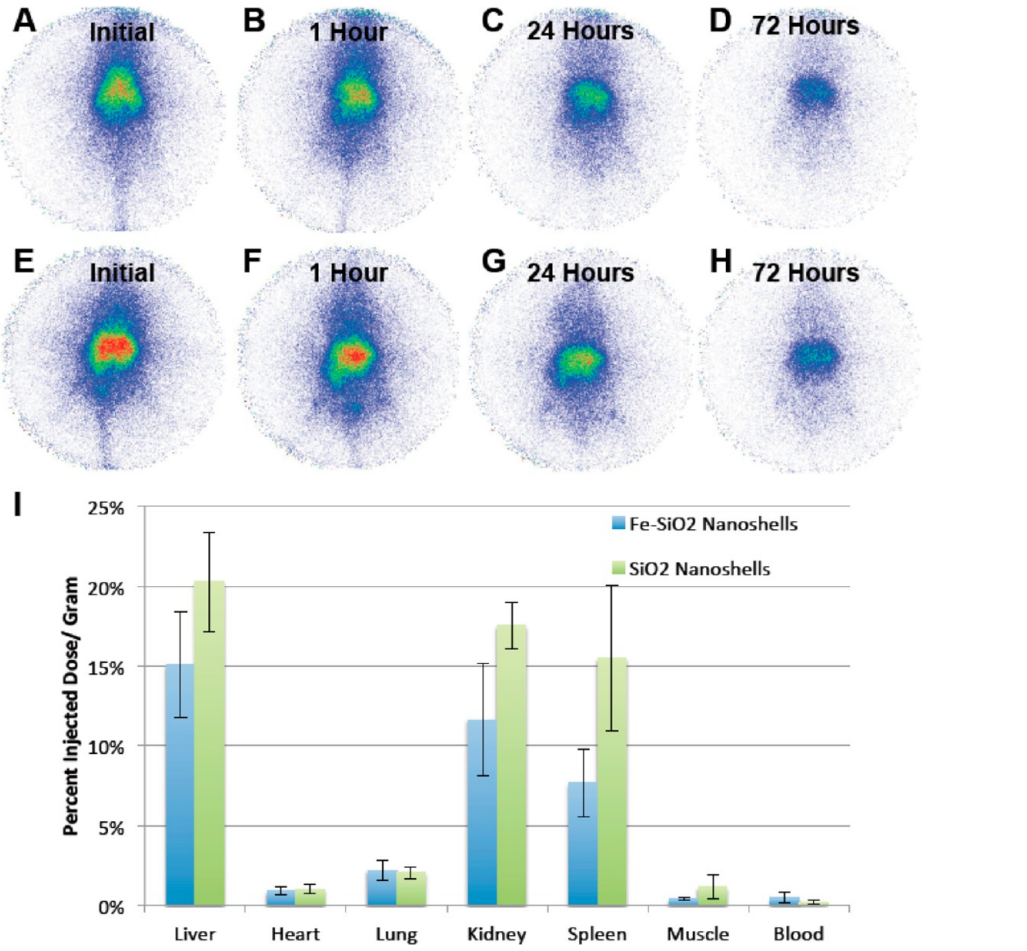

Figure 6. Biodistribution of radiolabeled 500 nm Fe−SiO_2 nanoshells in healthy nu/nu mice. Four healthy nu/nu mice were injected intravenously with 100 μL of ^{111}In labeled gas filled 500 nm Fe−SiO_2 nanoshells (A−D) and SiO_2 nanoshells (E−H) then imaged by gamma scinitigraphy. (A) Imaging during the injection. (B) Imaging 1 h postinjection. (C) Imaging 24 h postinjection. (D) Imaging 72 h postinjection. (E) Imaging at 0 h-during the injection. (F) Imaging 1 h postinjection. (G) Imaging 24 h postinjection. (H) Imaging 72 h postinjection. (I) Gamma counter readings of harvested organs for Fe−SiO_2 and SiO_2 nanoshells. Error bars are the standard deviations.

scintigraphy due to normalization against mass; however, quantification by γ-counting or scintigraphy showed the liver radioactivity was greater for both intratumoral and IV delivery. These results are consistent with the hypothesis that the intact 500 nm nanoparticles are taken up by the liver, but a small fraction of particles or released radiolabel and surface degraded products are retained by the renal system. The profiles of the distributions for both types of nanoshells (pure SiO_2 and Fe−SiO_2) are very similar; however, the remaining radioactivity for the biodegradable Fe−SiO_2 nanoshells remains consistently lower even in healthy animals. This is consistent with some surface degradation followed by release and clearance of the radiolabel since it was previously demonstrated in Figure 3 that some ultrasound signal is present after 10 days. Therefore, some nanoshells remain active *in vivo* within the Py8119 tumors 10 days after intratumoral delivery even though there may be partial surface degradation and loss of the surface anchored radiolabel.

CONCLUSIONS

This is the first report of the biodistribution for intratumoral injection of any biodegradable calcinated silica particle and the first report of a silica particle biodistribution determined using ^{111}In-DTPA labeling. It has been shown that the perfluoropentane gas filled nanoshells can be intratumorally injected and imaged intermittently by color Doppler ultrasound over the course of 10 days. The increase in ultrasound imaging lifetime from previous reports is attributed to the thicker shell, which results from the integration of iron into the silica shell, and leads to a slower rate for gas escape. Intravenous delivery of radioactive Fe−SiO_2-^{111}In-DTPA nanoshells and radioimaging shows rapid uptake by the liver, which is consistent with previous reports for injection of noncalcinated and calcinated silica particles. Some signal is observed in the kidneys, which has been observed previously for similar sized silica particles. Intratumoral injection results in most particles being retained by the tumor, and those that escape have a biodistribution similar to that

of IV injected particles. Biodistribution profiles of biodegradable Fe−SiO_2 nanoshells and SiO_2 nanoshells were similar with the exception of high liver retention of nonbiodegradable nanoshells in tumor bearing animals. This difference was not observed in healthy mice. Loss of radioactivity by the Fe−SiO_2 nanoshells is more pronounced and consistent with the effects of biodegradation. It has been hypothesized that the Fe−SiO_2 nanoshells degrade *via* a transferrin-mediated pathway,[30] and it is known that many cancers overexpress transferrin receptors,[49−51] which may accelerate Fe−SiO_2 nanoshell degradation. Alternatively, other models of cancer in murine models have shown that extrahepatic tumors cause significant changes in liver metabolism and drug retention. Such effects may play a role in the differences observed between the liver retention of Fe−SiO_2 nanoshells and SiO_2 nanoshells during IV administration to tumor bearing animals.[44−48] It is noteworthy that even during the initial IV injection of the nanoshells, accumulation in the tumors was detectable. Both SiO_2 and Fe−SiO_2 nanoshells passively accumulate as a function of tumor mass/vascularization, as evidenced by the roughly equal values of percent injected dose per gram tumor after intravenous delivery. It is hypothesized that the nanoparticles retained by the tumor after intravenous administration are a product of the enhanced permeation and retention effect.[41−43]

MATERIALS AND METHODS

Materials. Tetramethyl orthosilicate (TMOS) and 3-aminopropyl triethoxysilane (3-APTES) were purchased from Sigma-Aldrich (St. Louis, MO). Iron(III) ethoxide was obtained from Gelest Inc. (Moorisville, PA), 500 nm amino-polystyrene templates were provided by Polysciences (Warrington, PA). Perfluoropentane was purchased from Strem Chemicals (Newburyport, MA). 2-(4-Isothiocyanatobenzyl)-diethylenetriaminepentaacetic acid (p-SCN-Bn-DTPA) was purchased from Macrocyclics (Dallas,TX). $^{111}InCl_3$ was provided by Covidien (Mansfield, MA) in 0.1 N HCl. Milli-Q water purification undergoes multiple steps of filtration and deionization, which is measured by the resistivity of the water. A Millipore SuperQ Plus Water Purification System (Billerica, MA) was used to attain purified water.

The ultrasound imaging was performed with the Siemens Sequoia 512 (Mountainview, CA) with the Acuson 15L8 transducer that is commonly used for clinical US imaging. During imaging of the nanoshells, US parameters (frequency, focal depth, output power, filters and gains) were optimized in order to maximize signals from nanoshells while reducing background, which is a typical procedure in clinical contrast enhanced ultrasound (CEUS). Fluorescence imaging was performed by Ziess Axio Z1 fluorescence microscope. A CRC15 Dose Calibrator (Capintec, Inc., Ramsey, New Jersey) was used to measure doses as well as ^{111}In retention on DTPA functionalized particles. A high resolution gamma camera (γ1 Imager, BioSpace, Paris France) was used for planar scintigraphic imaging with a medium-energy high sensitivity collimator and dual energy windows set at 145−195 keV and 208−282 keV for detecting ^{111}In. Radioactivity of resected mouse organs was measured by an autowell gamma counter (Gamma 9000, Beckman Instruments, Fullerton CA).

Animals and Tumor Model. The 6-week-old female nu/nu mice were purchased from Charles River Laboratories and housed in a UCSD approved animal housing facility. Animals were fed Harlan Tecklad rodent feed and kept at 22 °C with a 12 h light/dark cycle. After an acclimation period of 10 days, 10^6 Py8119 breast cancer cells were injected subcutaneously and the resulting tumors were grown to 1000 mm^3 in volume. This cell line derived from the spontaneous polyomavirus middle T oncogene (PyVmT) mouse model of breast cancer represents the claudin low subtype of human breast cancer and has been previously used for surgical imaging studies.[52] Animals were scanned about two weeks after implantation, were anesthetized with isoflurane gas, and sacrificed by CO_2 asphyxiation post-experimentation.

Nanoshell Synthesis. Iron(III) ethoxide was first suspended in ethanol at a concentration of 20 mg/mL in an inert environment, and this solution was bath sonicated for 60 min. The iron ethoxide solution was mixed with pure TMOS at a ratio of 1:0.27 and was bath sonicated for an additional 10 min. This mixture was added to an Eppendorf tube with 500 nm amino-polystyrene templates in ethanol, which was subsequently pulse-vortexed at 3000 rpm for 5 h. After the reaction was complete, the particles were washed twice with ethanol by centrifugation to remove excess unreacted materials and left to dry overnight. Once dry, the particles were calcined at 550 °C for 18 h. There are approximately 7×10^9 nanoshells/mg after calcination. Nanoshells were stored dry until needed for gas filling or functionalization. Nanoshells were characterized by TEM and SEM as seen in Figure 1. Pure SiO_2 nanoshells were synthesized as previously described.[8,9,53] Nanoshell size distributions were determined from SEM images by individually measuring the diameters of 300 particles from multiple images in various fields of view using Image J for the Fe−SiO_2 and pure SiO_2 nanoshells.

Nanoshell Functionalization. Fe−SiO_2 nanoshells were suspended in ethanol at a concentration of 3 mg/mL in an Eppendorf tube. Separately, 1 μL of 3-APTES was added to 150 μL of ethanol in an Eppendorf tube, the solution was briefly mixed, and a 50 μL aliquot was removed and added to the nanoshell suspension. The nanoshells were pulse-vortexed at 3000 rpm for 24 h after which they were washed twice with ethanol and resuspended in DMSO. Then, 1 μL of 1 μg/mL of DTPA-isothiocyanate or 2 μL of 10 mg/mL of FITC was added to the nanoshells solution and pulse-vortexed for an additional 24 h. The nanoshells were washed twice with DMSO and once with ethanol. The nanoshells were dried and stored at 4 °C until needed. For pure silica nanoshells, the same processes were used, but the starting concentration was halved to account for differences in particle masses and retain an equivalent particle count.

Indium-111 Labeling. DTPA functionalized nanoshells were filled with perfluoropentane (PFP) as described previously[9] and suspended in 2.0 M sodium citrate solution at a concentration of 4 mg/mL (Fe−SiO_2) or 2 mg/mL (pure SiO_2). A 2 mg portion of the Fe−SiO_2 nanoshells or 1 mg of the SiO_2 nanoshells was pipetted into an Eppendorf tube and incubated with ~100 μC of indium-111 chloride for 30 min; 90% of the solution was removed from the Eppendorf tube and washed once with Milli-Q purified water and twice with ethanol. The nanoshells and the discarded supernatant were measured by dose calibrator in between each wash to track the indium retention on the nanoshells. After being washed, the nanoshells were dried under vacuum, filled with PFP gas, and suspended at a concentration of 4 mg/mL (Fe−SiO_2) or 2 mg/mL (SiO_2) in Milli-Q water.

***Ex Vivo* Doppler Ultrasound in Mastectomy Tissue.** IRB approval was obtained to test in human tissue from mastectomy patients with palpable tumors. The mastectomy specimens were imaged *ex vivo* using ultrasound B-mode to identify the tumor. Nanoshells were injected peritumorally under ultrasound guidance, and confirmation of particle injection was visualized by color Doppler ultrasound. Subsequently, the mastectomy specimen

was cut with the pathologist and a section of tumor and surrounding breast tissue was fixed in formalin. The needle used to inject the particles was left in place to guide the track of the particles. To better track and visualize the nanoshells under brightfield microscopy, the particles were suspended in a 10% (v/v) India ink solution. Additionally, nanoshells were covalently modified with fluorescein isothiocyanate (FITC) for fluorescent visualization.

Intratumoral Nanoshell Ultrasound Imaging Longevity. Eight Py8119 tumor bearing nu/nu mice were used to determine the *in vivo* ultrasound imaging longevity. For ultrasound imaging, each animal received a 50 μL injection of PFP-filled Fe$-$SiO$_2$ nanoshells directly into the tumor. The tumors were imaged intermittently with color Doppler ultrasound at an MI of 1.9 and a frequency of 7 MHz over the course of 14 days. The color Doppler signal width was measured from each imaging cycle and plotted over time.

Nanoshell Biodistribution in Py8119 Tumor Bearing nu/nu Mice. Four Py8119 tumor bearing nu/nu mice per group, each carrying two tumors on their posterior regions, were used to establish biodistribution when nanoshells were administered directly into a tumor or intravenously (four groups total). An amount of 100 μL of DTPA functionalized, ^{111}In labeled nanoshells was injected directly into a single tumor of each animal. Subsequent planar scintigraphic imaging was performed during the initial injection, 1 h postinjection, 24 h postinjection, and 72 h postinjection. Scintigraphic imaging time was preset to 15 min per imaging time point. The mice were sacrificed and the harvested organs were analyzed by gamma counter. For all scintigraphic images, the display range was fixed between 0 and 1.5.

Nanoshell Biodistribution in Healthy nu/nu Mice. Four healthy nu/nu mice per group were used to establish the biodistribution when nanoshells were administered intravenously to mimic the biodistribution of particles which might leak out of a small tumor after intratumoral (IT) injection. A 100 μL portion of DTPA functionalized, ^{111}In labeled nanoshells was injected *via* the tail vein. Subsequent planar scintigraphic imaging was performed during the initial injection, 1 h postinjection, 24 h postinjection, and 72 h postinjection. Scintigraphic imaging time was preset to 15 min per imaging time point. The mice were sacrificed, and the harvested organs were analyzed by gamma counter. For all scintigraphic images, the display range was fixed between 0 and 1.5.

Conflict of Interest: The authors declare no competing financial interest.

Acknowledgment. This study has been funded by the R21-CA151140. This study utilized the Small Animal Imaging Resource supported by the *In vivo* Cancer and Molecular Imaging Center (ICMIC) P50-CA128346. AL is supported by an R25 CA153915 training grant as well as R01CA095298 from the National Cancer Institute. The content is solely the responsibility of the authors and does not necessarily represent the official views of the National Cancer Institute or the National Institutes of Health. Z.W. is supported by a Career Development Award through the ICMIC and UCSD Academic Senate Grant RK131H. L. G.E. was supported by NCI Grant K22CA118182. The authors wish to thank Siemens Medical Solutions USA, Inc. for providing the Sequoia US system as equipment loans to UCSD. The authors acknowledge the use of the UCSD Cryo-Electron Microscopy Facility which is supported by NIH grants to Dr. Timothy S. Baker and a gift from the Agouron Institute to UCSD.

REFERENCES AND NOTES

1. Couleaud, P.; Morosini, V.; Frochot, C.; Richeter, S.; Raehm, L.; Durand, J.-O. Silica-Based Nanoparticles for Photodynamic Therapy Applications. *Nanoscale* **2010**, *2*, 1083–1095.
2. Lebret, V.; Raehm, L.; Durand, J.-O.; Smaihi, M.; Werts, M. H. V.; Blanchard-Desce, M.; Methy-Gonnod, D.; Dubernet, C. Folic Acid-Targeted Mesoporous Silica Nanoparticles for Two-Photon Fluorescence. *J. Biomed. Nanotechnol.* **2010**, *6*, 176–180.
3. Rieter, W. J.; Kim, J. S.; Taylor, K. M. L.; An, H.; Lin, W.; Tarrant, T.; Lin, W. Hybrid Silica Nanoparticles for Multimodal Imaging. *Angew. Chem., Int. Ed.* **2007**, *46*, 3680–3682.
4. Lin, Y.-S.; Hung, Y.; Su, J.-K.; Lee, R.; Chang, C.; Lin, M.-L.; Mou, C.-Y. Gadolinium(III)-Incorporated Nanosized Mesoporous Silica as Potential Magnetic Resonance Imaging Contrast Agents. *J. Phys. Chem. B* **2004**, *108*, 15608–15611.
5. Hsiao, J.-K.; Tsai, C.-P.; Chung, T.-H.; Hung, Y.; Yao, M.; Liu, H.-M.; Mou, C.-Y.; Yang, C.-S.; Chen, Y.-C.; Huang, D.-M. Mesoporous Silica Nanoparticles as a Delivery System of Gadolinium for Effective Human Stem Cell Tracking. *Small* **2008**, *4*, 1445–1452.
6. Yang, J.; Sandoval, S.; Alfaro, J. G.; Aschemeyer, S.; Liberman, A.; Martin, D. T.; Makale, M.; Kummel, A. C.; Trogler, W. C. Red-Luminescent Europium (III) Doped Silica Nanoshells: Synthesis, Characterization, and their Interaction with HeLa Cells. *J. Biomed. Opt.* **2011**, *16*, 066012.
7. Lu, J.; Liong, M.; Li, Z.; Zink, J. I.; Tamanoi, F. Biocompatibility, Biodistribution, and Drug-Delivery Efficiency of Mesoporous Silica Nanoparticles for Cancer Therapy in Animals. *Small* **2010**, *6*, 1794–1805.
8. Liberman, A.; Martinez, H. P.; Ta, C. N.; Barback, C. V.; Mattrey, R. F.; Kono, Y.; Blair, S. L.; Trogler, W. C.; Kummel, A. C.; Wu, Z. Hollow Silica and Silica-Boron Nano/Microparticles for Contrast-Enhanced Ultrasound to Detect Small Tumors. *Biomaterials* **2012**, *33*, 5124–5129.
9. Martinez, H. P.; Kono, Y.; Blair, S. L.; Sandoval, S.; Wang-Rodriguez, J.; Mattrey, R. F.; Kummel, A. C.; Trogler, W. C. Hard Shell Gas-Filled Contrast Enhancement Particles for Colour Doppler Ultrasound Imaging of Tumors. *Medchemcomm* **2010**, *1*, 266–270.
10. Ta, C. N.; Liberman, A.; Paul Martinez, H.; Barback, C. V.; Mattrey, R. F.; Blair, S. L.; Trogler, W. C.; Kummel, A. C.; Wu, Z. Integrated Processing of Contrast Pulse Sequencing Ultrasound Imaging for Enhanced Active Contrast of Hollow Gas Filled Silica Nanoshells and Microshells. *J. Vac. Sci. Technol., B* **2012**, *30*, 02C104–02C104–6.
11. Wang, X.; Chen, H.; Chen, Y.; Ma, M.; Zhang, K.; Li, F.; Zheng, Y.; Zeng, D.; Wang, Q.; Shi, J. Perfluorohexane-Encapsulated Mesoporous Silica Nanocapsules as Enhancement Agents for Highly Efficient High Intensity Focused Ultrasound (HIFU). *Adv. Mater.* **2012**, *24*, 785–791.
12. Hu, H.; Zhou, H.; Du, J.; Wang, Z.; An, L.; Yang, H.; Li, F.; Wu, H.; Yang, S. Biocompatiable Hollow Silica Microspheres as Novel Ultrasound Contrast Agents for *in Vivo* Imaging. *J. Mater. Chem.* **2011**, *21*, 6576–6583.
13. Lin, P.-L.; Eckersley, R. J.; Hall, E. A. H. Ultrabubble: A Laminated Ultrasound Contrast Agent with Narrow Size Range. *Adv. Mater.* **2009**, *21*, 3949–3952.
14. Krekel, N.; Zonderhuis, B.; Muller, S.; Bril, H.; van Slooten, H.-J.; de Lange de Klerk, E.; van den Tol, P.; Meijer, S. Excessive Resections in Breast-Conserving Surgery: A Retrospective Multicentre Study. *Breast* **2011**, *17*, 602–609.
15. Rahusen, F. D.; Bremers, A. J. A.; Fabry, H. F. J.; Taets van Amerongen, A. H. M.; Boom, R. P. A.; Meijer, S. Ultrasound-Guided Lumpectomy of Nonpalpable Breast Cancer *versus* Wire-Guided Resection: A Randomized Clinical Trial. *Ann. Surg. Oncol.* **2002**, *9*, 994–998.
16. Gray, R. J.; Pockaj, B. A.; Karstaedt, P. J.; Roarke, M. C. Radioactive Seed Localization of Nonpalpable Breast Lesions Is Better than Wire Localization. *Am. J. Surg.* **2004**, *188*, 377–380.
17. Hughes, J. H.; Mason, M. C.; Gray, R. J.; McLaughlin, S. A.; Degnim, A. C.; Fulmer, J. T.; Pockaj, B. A.; Karstaedt, P. J.; Roarke, M. C.; Multi-site, A. Validation Trial of Radioactive Seed Localization as an Alternative to Wire Localization. *Breast* **2008**, *14*, 153–157.
18. Regelsberger, J.; Lohmann, F.; Helmke, K.; Westphal, M. Ultrasound-Guided Surgery of Deep Seated Brain Lesions. *Eur. J. Ultrasound* **2000**, *12*, 115–121.
19. Torzilli, G.; Takayama, T.; Hui, A.-M.; Kubota, K.; Harihara, Y.; Makuuchi, M. A New Technical Aspect of Ultrasound-Guided Liver Surgery. *Am. J. Surg.* **1999**, *178*, 341–343.
20. Harlow, S. P.; Krag, D. N.; Ames, S. E.; Weaver, D. L. Intraoperative Ultrasound Localization to Guide Surgical Excision of Nonpalpable Breast Carcinoma. *J. Am. Coll. Surg.* **1999**, *189*, 241–246.

21. Dogan, B. E.; Whitman, G. J. Intraoperative Breast Ultrasound. *Semin. Roentgenol.* **2011**, *46*, 280–284.
22. Han, J. S.; Molberg, K. H.; Sarode, V. Predictors of Invasion and Axillary Lymph Node Metastasis in Patients with a Core Biopsy Diagnosis of Ductal Carcinoma *in Situ*: An Analysis of 255 Cases. *Breast* **2011**, *17*, 223–229.
23. He, X.; Nie, H.; Wang, K.; Tan, W.; Wu, X.; Zhang, P. *In Vivo* Study of Biodistribution and Urinary Excretion of Surface-Modified Silica Nanoparticles. *Anal. Chem.* **2008**, *80*, 9597–9603.
24. Liu, T.; Li, L.; Teng, X.; Huang, X.; Liu, H.; Chen, D.; Ren, J.; He, J.; Tang, F. Single and Repeated Dose Toxicity of Mesoporous Hollow Silica Nanoparticles in Intravenously Exposed Mice. *Biomaterials* **2011**, *32*, 1657–1668.
25. Decuzzi, P.; Godin, B.; Tanaka, T.; Lee, S. Y.; Chiappini, C.; Liu, X.; Ferrari, M. Size and Shape Effects in the Biodistribution of Intravascularly Injected Particles. *J. Controlled Release* **2010**, *141*, 320–327.
26. Kommareddy, S.; Amiji, M. Biodistribution and Pharmacokinetic Analysis of Long-Circulating Thiolated Gelatin Nanoparticles Following Systemic Administration in Breast Cancer-Bearing Mice. *J. Pharm. Sci.* **2007**, *96*, 397–407.
27. Zhang, R.; Xiong, C.; Huang, M.; Zhou, M.; Huang, Q.; Wen, X.; Liang, D.; Li, C. Peptide-Conjugated Polymeric Micellar Nanoparticles for Dual SPECT and Optical Imaging of EphB4 Receptors in Prostate Cancer Xenografts. *Biomaterials* **2011**, *32*, 5872–5879.
28. Melancon, M. P.; Lu, W.; Yang, Z.; Zhang, R.; Cheng, Z.; Elliot, A. M.; Stafford, J.; Olson, T.; Zhang, J. Z.; Li, C. *In Vitro* and *In Vivo* Targeting of Hollow Gold Nanoshells Directed at Epidermal Growth Factor Receptor for Photothermal Ablation Therapy. *Mol. Cancer Ther.* **2008**, *7*, 1730–1739.
29. Tsai, C.-P.; Hung, Y.; Chou, Y.-H.; Huang, D.-M.; Hsiao, J.-K.; Chang, C.; Chen, Y.-C.; Mou, C.-Y. High-Contrast Paramagnetic Fluorescent Mesoporous Silica Nanorods as a Multifunctional Cell-Imaging Probe. *Small* **2008**, *4*, 186–191.
30. Mitchell, K. K. P., Iron(III)-Doped, Silica: Biodegradable, Self-Targeting Nanoparticles. UCSD: 2011; Vol. Thesis Dissertation.
31. Pohaku Mitchell, K. K.; Liberman, A.; Kummel, A. C.; Trogler, W. C. Iron(III)-Doped, Silica Nanoshells: A Biodegradable Form of Silica. *J. Am. Chem. Soc.* **2012**, *134*, 13997–14003.
32. Yu, T.; Malugin, A.; Ghandehari, H. Impact of Silica Nanoparticle Design on Cellular Toxicity and Hemolytic Activity. *ACS Nano* **2011**, *5*, 5717–5728.
33. Hermanson, G. *Bioconjugate Techniques*; Academic Press: San Diego, CA, 1996.
34. Kobler, J.; Möller, K.; Bein, T. Colloidal Suspensions of Functionalized Mesoporous Silica Nanoparticles. *ACS Nano* **2008**, *2*, 791–799.
35. Ng, C. P.; Pun, S. H. A Perfusable 3D Cell–Matrix Tissue Culture Chamber for *in Situ* Evaluation of Nanoparticle Vehicle Penetration and Transport. *Biotechnol. Bioeng.* **2008**, *99*, 1490–1501.
36. Longmire, M.; Choyke, P. L.; Kobayashi, H. Clearance Properties of Nano-Sized Particles and Molecules as Imaging Agents: Considerations and Caveats. *Nanomedicine* **2008**, *3*, 703–717.
37. Paik, C. H.; Quadri, S. M.; Reba, R. C. Interposition of Different Chemical Linkages between Antibody and ^{111}In-DTPA To Accelerate Clearance from Non-Target Organs and Blood. *Int. J. Rad. Appl. Instrum. B.* **1989**, *16*, 475–481.
38. Prata, M. I. M.; Santos, A. C.; Bligh, S. W. A.; Chowdhury, A. H. M. S.; Geraldes, C. F. G. C.; de Lima, J. J. P. Characterization of $^{111}In^{3+}$ Complexes of DTPA Amide Derivatives: Biodistribution and Clearance Studied by Gamma Imaging. *Nucl. Med. Biol.* **2000**, *27*, 605–610.
39. Li, C.; Yu, D.-F.; Inoue, T.; Yang, D. J.; Tansey, W.; Liu, C.-W.; Milas, L.; Hunter, N. R.; Kim, E. E.; Wallace, S. Synthesis, Biodistribution and Imaging Properties of Indium-111-DTPA-Paclitaxel in Mice Bearing Mammary Tumors. *J. Nucl. Med.* **1997**, *38*, 1042–1047.
40. Lilien, D. L.; Berger, H. G.; Anderson, D. P.; Bennett, L. R. ^{111}In-Chloride: A New Agent for Bone Marrow Imaging. *J. Nucl. Med.* **1973**, *14*, 184–186.
41. Maeda, H.; Wu, J.; Sawa, T.; Matsumura, Y.; Hori, K. Tumor Vascular Permeability and the EPR Effect in Macromolecular Therapeutics: A Review. *J. Controlled Release* **2000**, *65*, 271–284.
42. Son, Y. J.; Jang, J.-S.; Cho, Y. W.; Chung, H.; Park, R.-W.; Kwon, I. C.; Kim, I.-S.; Park, J. Y.; Seo, S. B.; Park, C. R.; *et al.* Biodistribution and Anti-Tumor Efficacy of Doxorubicin Loaded Glycol-Chitosan Nanoaggregates by EPR Effect. *J. Controlled Release* **2003**, *91*, 135–145.
43. Davis, M. E.; Chen, Z.; Shin, D. M. Nanoparticle Therapeutics: An Emerging Treatment Modality for Cancer. *Nat. Rev. Drug Discov.* **2008**, *7*, 771–782.
44. Lee, A.; Chick, J. M.; Kolarich, D.; Haynes, P. A.; Robertson, G. R.; Tsoli, M.; Jankova, L.; Clarke, S. J.; Packer, N. H.; Baker, M. S., Liver Membrane Proteome Glycosylation Changes in Mice Bearing an Extra-Hepatic Tumor. *Mol. Cell. Proteomics* **2011**, *10*.
45. Kacevska, M.; Downes, M. R.; Sharma, R.; Evans, R. M.; Clarke, S. J.; Liddle, C.; Robertson, G. R. Extrahepatic Cancer Suppresses Nuclear Receptor–Regulated Drug Metabolism. *Clin. Cancer. Res.* **2011**, *17*, 3170–3180.
46. Kacevska, M.; Mahns, A.; Sharma, R.; Clarke, S.; Robertson, G.; Liddle, C. Extra-Hepatic Cancer Represses Hepatic Drug Metabolism *via* Interleukin (IL)-6 Signalling. *Pharm. Res.* **2013**, 1–9.
47. Sharma, R.; Kacevska, M.; London, R.; Clarke, S. J.; Liddle, C.; Robertson, G. Downregulation of Drug Transport and Metabolism in Mice Bearing Extra-Hepatic Malignancies. *Br. J. Cancer* **2007**, *98*, 91–97.
48. Kacevska, M.; Robertson, G. R.; Clarke, S. J.; Liddle, C. Inflammation and CYP3A4-Mediated Drug Metabolism in Advanced Cancer: Impact and Implications for Chemotherapeutic Drug Dosing. *Expert Opin Drug Metab Toxicol* **2008**, *4*, 137–149.
49. Hogemann-Savellano, D.; Bos, E.; Blondet, C.; Sato, F.; Abe, T.; Josephson, L.; Weissleder, R.; Gaudet, J.; Sgroi, D.; Peters, P. J.; et al. The Transferrin Receptor: A Potential Molecular Imaging Marker for Human Cancer. *Neoplasia* **2003**, *5*, 495–506.
50. Shindelman, J. E.; Ortmeyer, A. E.; Sussman, H. H. Demonstration of the Transferrin Receptor in Human Breast Cancer Tissue. Potential Marker for Identifying Dividing Cells. *Int. J. Cancer* **1981**, *27*, 329–334.
51. Page Faulk, W.; Hsi, B.-L.; Stevens, P. J. Transferrin and Transferrin Receptors in Carcinoma of the Breast. *Lancet* **1980**, *316*, 390–392.
52. Nguyen, Q. T.; Olson, E. S.; Aguilera, T. A.; Jiang, T.; Scadeng, M.; Ellies, L. G.; Tsien, R. Y. Surgery with Molecular Fluorescence Imaging Using Activatable Cell-Penetrating Peptides Decreases Residual Cancer and Improves Survival. *Proc. Natl. Acad. Sci. U.S.A.* **2010**, *107*, 4317–4322.
53. Yang, J.; Lind, J. U.; Trogler, W. C. Synthesis of Hollow Silica and Titania Nanospheres. *Chem. Mater.* **2008**, *20*, 2875–2877.